

*Supplementary information for*

**Phosphate speciation on Al-substituted goethite: ATR-FTIR  
/2D-COS and CD-MUSIC modeling**

Jinling Xu<sup>1, 2</sup>, Luuk K. Koopal<sup>1, 3</sup>, Mingxia Wang<sup>1\*</sup>, Juan Xiong<sup>1</sup>, Jingtao Hou<sup>1</sup>, Yan  
Li<sup>1</sup>, Wenfeng Tan<sup>1, 2\*</sup>

<sup>1</sup> Key Laboratory of Arable Land Conservation (Middle and Lower Reaches of Yangtze River), Ministry of Agriculture, College of Resources and Environment, Huazhong Agricultural University, Wuhan 430070, P. R. China

<sup>2</sup> State Key Laboratory of Soil Erosion and Dryland Farming on the Loess Plateau, Institute of Soil and Water Conservation, Chinese Academy of Sciences and the Ministry of Water Resources, Yangling, Shaanxi Province 712100, P. R. China

<sup>3</sup> Physical Chemistry and Soft Matter, Wageningen University and Research, Stippeneng 4, 6708 WE Wageningen, The Netherlands.

\* Corresponding authors

tanwf@mail.hzu.edu.cn and wangmx@mail.hzau.edu.cn

## Contents

Dissolution kinetics (Fig. S1, Table S1) .....	S3
Proton charge densities at different KNO <sub>3</sub> concentration.....	S6
Phosphate adsorption edges .....	S7
Table S2 Reactive site densities on the predominant crystal faces of goethite.....	S8
Fig. S2 Schematic representation of (110) and (021) face of Al-substituted goethite .....	S9
Fig. S3 Inner-sphere phosphate complexes on Al-substituted goethite .....	S10
Table S3 The basic surface species, charge allocation ( $\Delta z$ ), stoichiometric coefficients, and affinity constants ( $\log K$ ) of H <sup>+</sup> , K <sup>+</sup> , and NO <sub>3</sub> <sup>-</sup> interacting with singly and triply reactive surface groups on Al-substituted goethite surface .....	S11
X-ray diffraction results (Fig. S4 and S5) .....	S12
Fig. S6 SEM images of goethite and Al-substituted goethites .....	S13
Fig. S7 Histograms of particle length and width distributions of the goethites.....	S14
Fig. S8 Time-dependent ATR-FTIR spectra of adsorbed phosphate.....	S15
Two-dimensional correlation spectra (2D-COS) of phosphate adsorption (Fig. S9, S10; Tables S4, S5) .....	S16
The sensitivity analysis of the fitting of surface charge data.....	S22
References.....	S24

## Dissolution kinetics

**Aim.** Analysis of the dissolution kinetics of Fe and Al upon dissolution of Al-substituted goethite provides important information concerning the homogeneity of Al within crystals of goethite <sup>1,2</sup>. Therefore, dissolution experiments in acidic solution at 55 °C of Al-substituted goethite were carried out as a function of time.

**Experiments.** An accurately weighed 0.100 g of G-0, G-6 and G-9 were each suspended in 250 mL of 6 M HCl and sealed in a cylindrical beaker that was thermostatted at 55 °C with a water bath. The experiments were carried out under continuous stirring at a constant rate. The dissolution behavior was examined by quantifying the amount of Fe and Al released by withdrawing, at predetermined time intervals, 5 mL aliquots of the suspension, which were filtered through 0.22 µm membranes. Quantification of dissolved Fe and Al was performed by inductively coupled plasma emission spectroscopy (ICP-OES).

**Results.** The Fe dissolution of G-0, G-6 and G-9 is depicted in Fig. S1a as the fraction of Fe dissolved vs. time. Considerable differences between the curves were observed: pure goethite dissolved most rapidly and the rate of goethite dissolution decreased with increasing Al content. The Fe dissolution kinetics could be described well by the linearized Kabai equation <sup>3</sup>:

$$\ln \ln \left( \frac{1}{1 - \chi_{Fe}} \right) = \alpha \ln k + \alpha \ln t \quad (S1)$$

where  $\chi_{\text{Fe}}$  is the fraction of Fe dissolved at time  $t$ ;  $\alpha$  represents a constant that is characteristic of the solid phase and  $k$  is the dissolution rate constant. The fitted parameters are tabulated in Table S1.

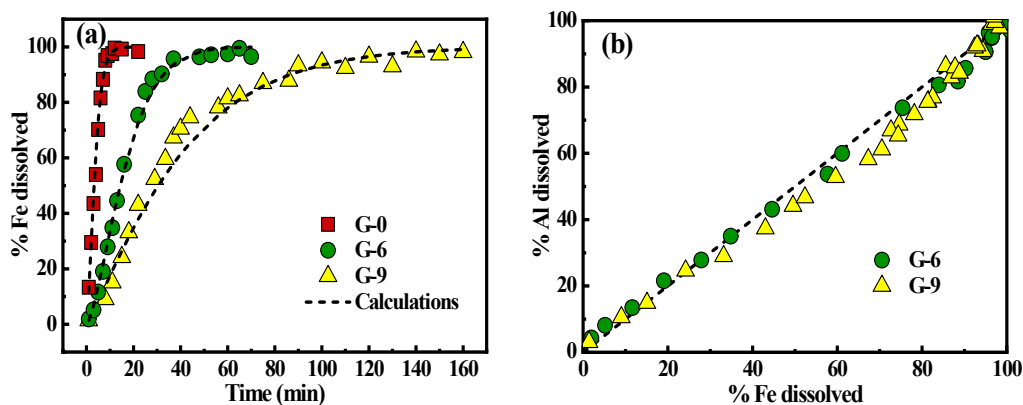


**Fig. S1** G-0, G-6 and G-9 dissolution in 6 M HCl at 55 °C: (a) % Fe dissolved vs. time; the symbols are experimental data, and the dashed lines describe the dissolution according to eq. S1 using the (fitted) parameters shown in Table S1; (b) Congruency of dissolution plotted as % Al dissolved vs. % Fe dissolved.

**Table S1** Dissolution parameters derived from eq. S1

Sample	$N$	$\alpha$	$k/\text{min}^{-1}$	$R^2$
G-0	13	1.465	0.242	0.989
G-6	18	1.465	0.054	0.989
G-9	24	1.151	0.024	0.981

$N$  represents the number of experimental points.  $\alpha$  is a constant that is characteristic of the solid phase and  $k$  is the Fe dissolution rate constant ( $\text{min}^{-1}$ ).

The Fe dissolution rate constant  $k$  of pure goethite ( $0.242 \text{ min}^{-1}$ ) is 9-fold larger than that of G-9 ( $0.024 \text{ min}^{-1}$ ), indicating a significant effect of Al substitution on the stability against proton attack. According to Schwertmann (1984)<sup>4</sup> Al affects the dissolution rate of goethite by influencing crystal size and order which are related to

the effect of Al on the crystal growth rate. In addition, the substitution of  $\text{Al}^{3+}$  for  $\text{Fe}^{3+}$  causes a shortening and strengthening of the Me-O or Me-OH bonds, which may also influence the dissolution rate <sup>5</sup>. In Fig. S1b dissolved Al (%) is depicted as a function of dissolved Fe (%). The dashed line with unit slope indicates complete congruency of the Al and Fe dissolution. The results indicate that the dissolution is nearly congruent, suggesting that Al is distributed nearly uniformly throughout the goethite crystals. The result agrees with a previous study that for Al contents around 10 mol%, Al atoms can be considered as isolated rather than Al clusters <sup>6</sup>.

### **Proton charge densities at different KNO<sub>3</sub> concentration**

The surface charge of goethite was determined by acid-base potentiometric titrations at  $25 \pm 0.1$  °C under a stable N<sub>2</sub> gas atmosphere using an automated titration setup (Metrohm, 836 Titrando). Two burettes (Metrohm, Dosimat) filled with 0.05 M KOH and HNO<sub>3</sub>, respectively, were used as titrants. The titration cell was filled with 50 mL 5 g/L goethite in 0.005 M KNO<sub>3</sub>. During the titration the pH in the solution was monitored with a combined-pH electrode (Metrohm, 6.0262.100). Prior to the titration the suspension was adjusted to approximately pH 4 and purged with N<sub>2</sub> gas for 2 h in order to remove possible CO<sub>2</sub> contamination. Subsequently, the pH of the suspension was kept constant within a tolerance range of 0.004 pH units (0.2 mV) to fully equilibrate the suspension. Incremental additions of base (up to about pH 10) and acid (back to about pH 4) were carried out at three salt concentrations (0.005 M, 0.03 M and 0.1 M KNO<sub>3</sub>). Blank titrations were also performed at the three salt concentrations to calibrate the equation for the theoretical blanks <sup>7</sup>. A pH-stat titration at pH 5.0 was made to determine the positions of the charge density vs. pH curves at the three salt concentrations with respect to each other. The thus obtained charge vs. pH curves intersect at a common intersection point that is equal to the pristine PZC. By putting the charge density at pH (PZC) equal to zero the absolute charge density curves are obtained. The procedure of the titrations and the calculations are described in more detail by Tan et al. (2008) <sup>7</sup> (procedure for humic acids is analogous to that for metal (hydr)oxides except for the determination of the PZC).

## Phosphate adsorption edges

Phosphate adsorption on the goethite samples was determined in batch experiments as a function of pH and phosphate concentration, using 0.01 and 0.1 M  $\text{KNO}_3$  as background electrolyte. A 10 g/L goethite stock suspension was prepared in either 0.01 or 0.1 M  $\text{KNO}_3$  at about pH 4. Prior to the adsorption experiments, the suspension and phosphate solutions were purged with  $\text{N}_2$  gas to remove possible  $\text{CO}_2$  contamination. To tubes containing 10 mL of 10 g/L goethite suspension, 10 mL of 3 mM or 0.9 mM  $\text{KH}_2\text{PO}_4$  prepared in 0.01 or 0.1 M  $\text{KNO}_3$  solution were added, resulting in a final goethite concentration of 5 g/L and a total initial phosphate concentration of 1.5 mM or 0.45 mM respectively. Small doses of 0.05 M, 0.1 M and 0.5 M  $\text{HNO}_3$  or  $\text{KOH}$  were added to adjust the pH to desired values. The prepared suspensions were shaken at 25 °C for 48 h; during the time, the pH of the suspensions was readjusted 2 to 3 times to the initial pH values under flushing with  $\text{N}_2$ . The final pH of the suspensions was recorded. Finally, the suspensions were centrifuged at 10,000 g and filtered using 0.22  $\mu\text{m}$  polyethersulfone membrane filters. The phosphate concentration in the supernatants was determined by the molybdenum-blue method<sup>8</sup>, and the extent of adsorption was calculated from the difference between the initial and final concentration of phosphate.

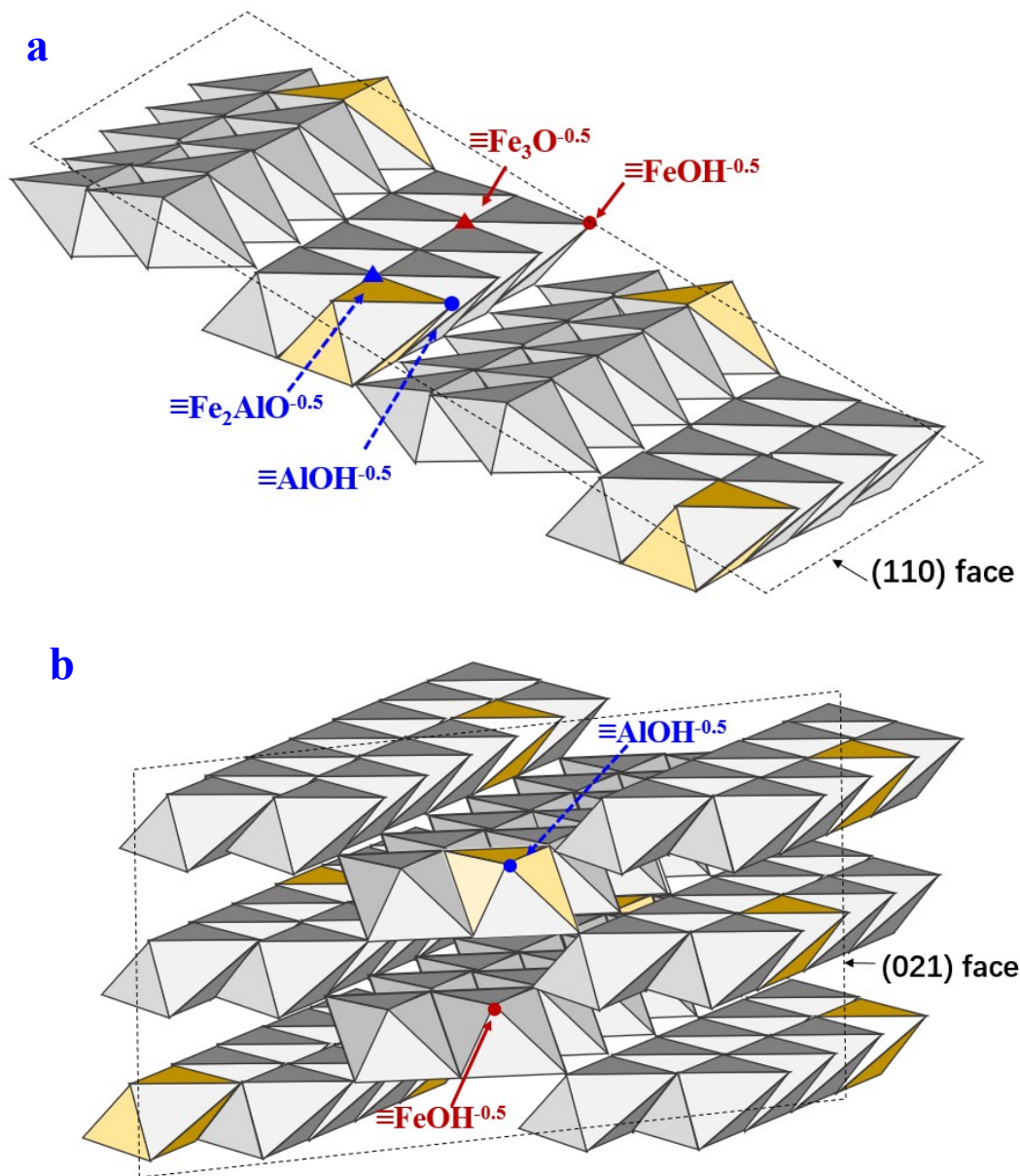
## Reactive site densities on the predominant crystal faces of goethite

**Table S2** Reactive site densities (sites/nm<sup>2</sup>) of singly and triply coordinated sites on the predominant crystal faces of goethite

Site type	(110) face $N_s$ (sites/nm <sup>2</sup> )	(021) face $N_s$ (sites/nm <sup>2</sup> )
Singly	3.03	7.5
Triply	3.03	0

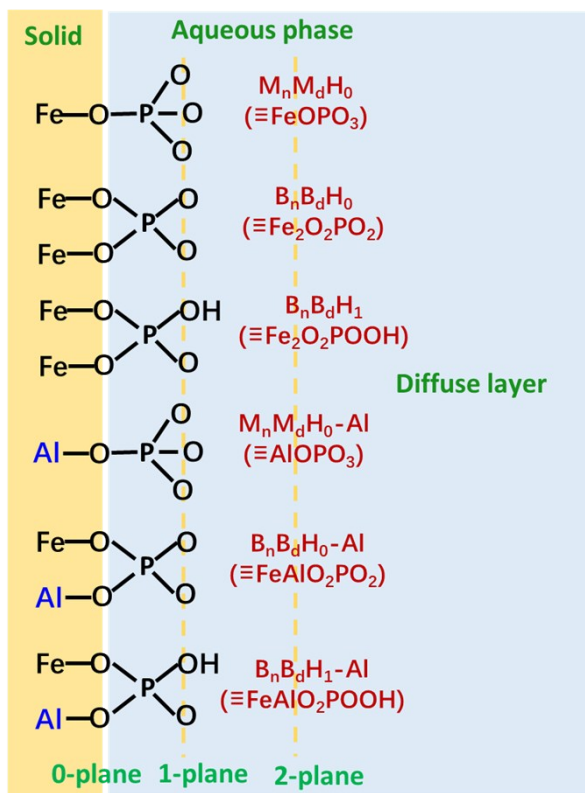
The data is taken from Venema et al. (1998) <sup>9</sup>.

Fig. S2 Schematic representation of the (110) and (021) faces of Al-substituted goethite



A schematic representation of the (110) face and (021) face of Al-substituted goethite using Fe-filled (grey) and Al-filled (yellow) octahedra.

Fig. S3 Inner-sphere phosphate complexes on Al-substituted goethite



Schematic picture of the Al-substituted goethite/water interface with adsorbed inner-sphere phosphate complexes. The 2-plane is the start of the diffuse layer.

**Table S3** The basic surface species, charge allocation ( $\Delta z$ ), stoichiometric coefficients, and affinity constants ( $\log K$ ) of  $H^+$ ,  $K^+$ , and  $NO_3^-$  interacting with singly and triply reactive surface groups on Al-substituted goethite surface

Surface species	$\equiv FeOH^{-0.5}$	$\equiv Fe_3O^{-0.5}$	$\equiv AlOH^{-0.5}$	$\equiv Fe_2AlO^{-0.5}$	${}^a \Delta z_0$	${}^a \Delta z_1$	${}^a \Delta z_2$	${}^a \log K$
$\equiv FeOH^{-0.5}$	1				0	0	0	0
$\equiv FeOH_2^{+0.5}$	1				+1	0	0	$\log K_H(\equiv FeOH^{-0.5})$
$\equiv FeOH^{-0.5} \dots K^+$	1				0	0	+1	-0.38
$\equiv FeOH_2^{+0.5} \dots NO_3^-$	1				+1	-0.7	-0.3	$\log K_H(\equiv FeOH^{-0.5}) - 0.43$
$\equiv Fe_3O^{-0.5}$		1			0	0	0	0
$\equiv Fe_3OH^{+0.5}$		1			+1	0	0	$\log K_H(\equiv Fe_3O^{-0.5})$
$\equiv Fe_3O^{-0.5} \dots K^+$		1			0	0	+1	-0.38
$\equiv Fe_3OH^{+0.5} \dots NO_3^-$		1			+1	-0.7	-0.3	$\log K_H(\equiv Fe_3O^{-0.5}) - 0.43$
$\equiv AlOH^{-0.5}$			1		0	0	0	0
$\equiv AlOH_2^{+0.5}$			1		+1	0	0	$\log K_H(\equiv AlOH^{-0.5})$
$\equiv AlOH^{-0.5} \dots K^+$			1		0	0	+1	-0.38
$\equiv AlOH_2^{+0.5} \dots NO_3^-$			1		+1	-0.7	-0.3	$\log K_H(\equiv AlOH^{-0.5}) - 0.43$
$\equiv Fe_2AlO^{-0.5}$				1	0	0	0	0
$\equiv Fe_2AlOH^{+0.5}$				1	+1	0	0	$\log K_H(\equiv Fe_2AlO^{-0.5})$
$\equiv Fe_2AlO^{-0.5} \dots K^+$				1	0	0	+1	-0.38
$\equiv Fe_2AlOH^{+0.5} \dots NO_3^-$				1	+1	-0.7	-0.3	$\log K_H(\equiv Fe_2AlO^{-0.5}) - 0.43$

<sup>a</sup> Data is from Rahnemaie et al. (2006)<sup>10</sup>.  $\Delta z_0$ ,  $\Delta z_1$ , and  $\Delta z_2$  represent the change of the charge at respectively 0-, 1-, and 2- planes; and  $\log K$  represents the affinity constant for protons or electrolyte ions.

## X-ray diffraction results

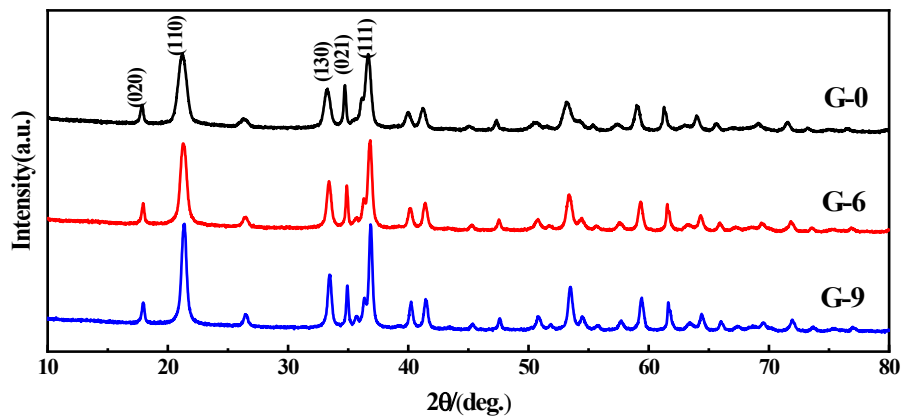


Fig. S4 XRD patterns of pure and Al-substituted goethite samples

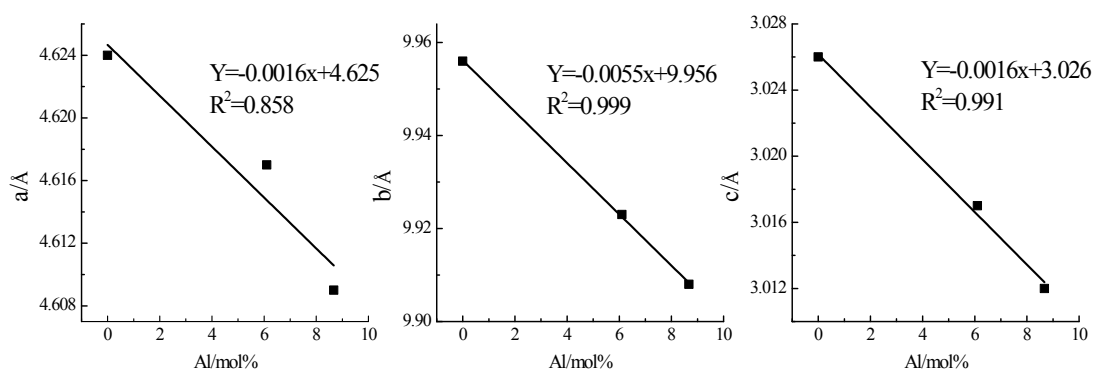
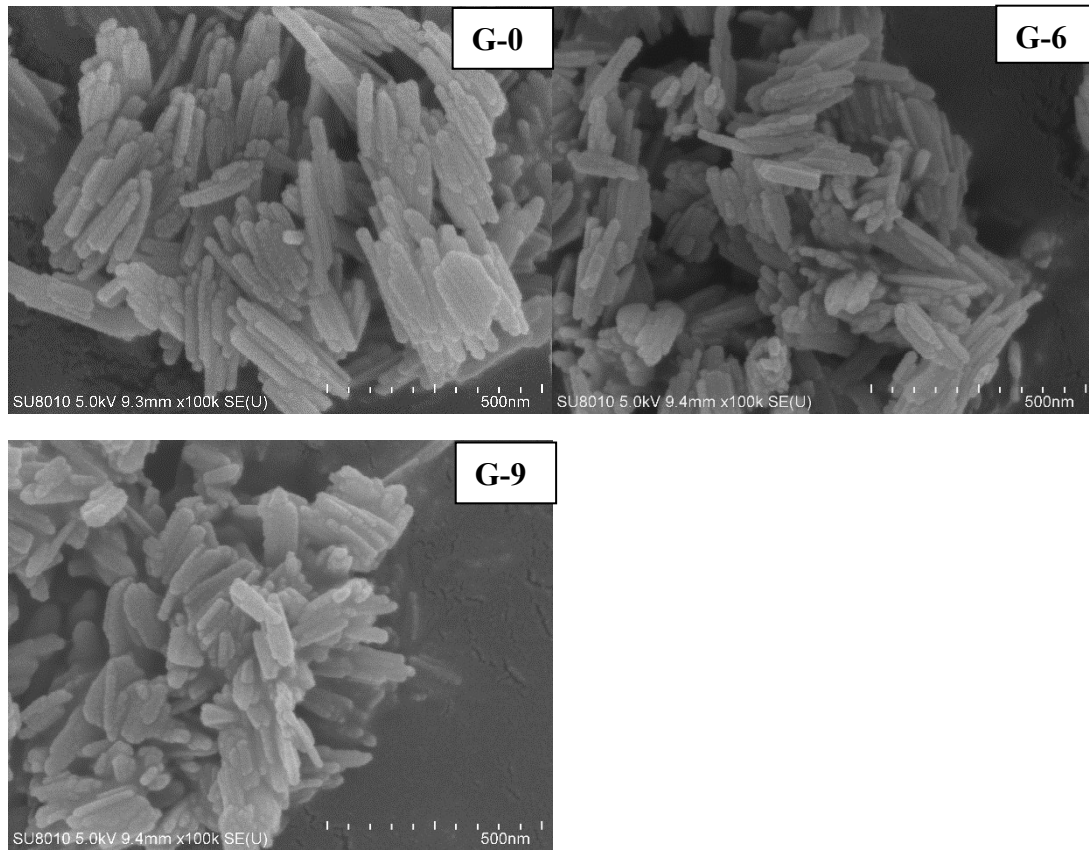
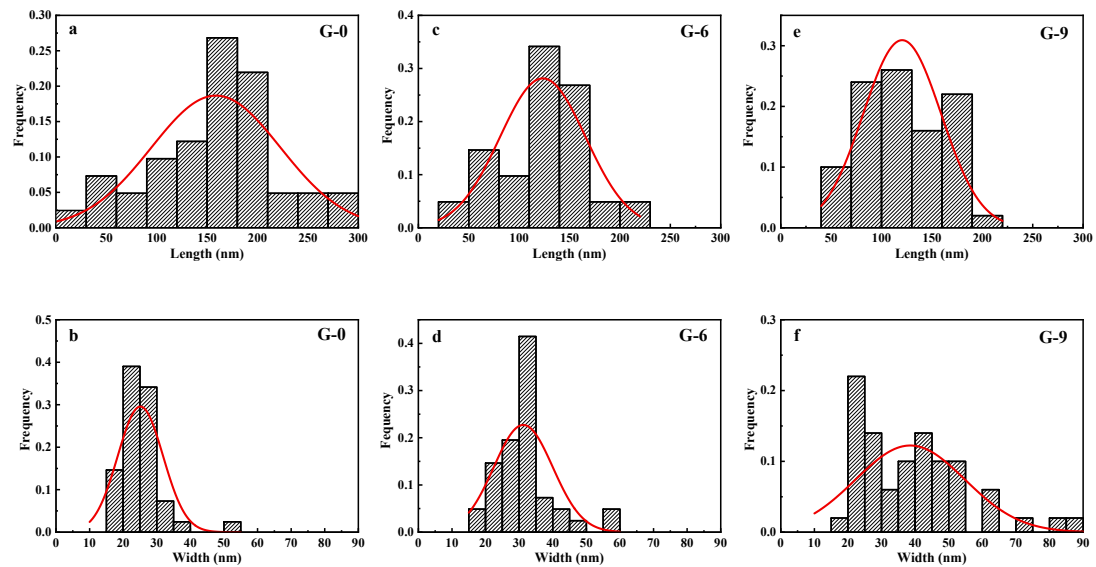


Fig. S5 Linear relationship between unit cell dimensions and Al content

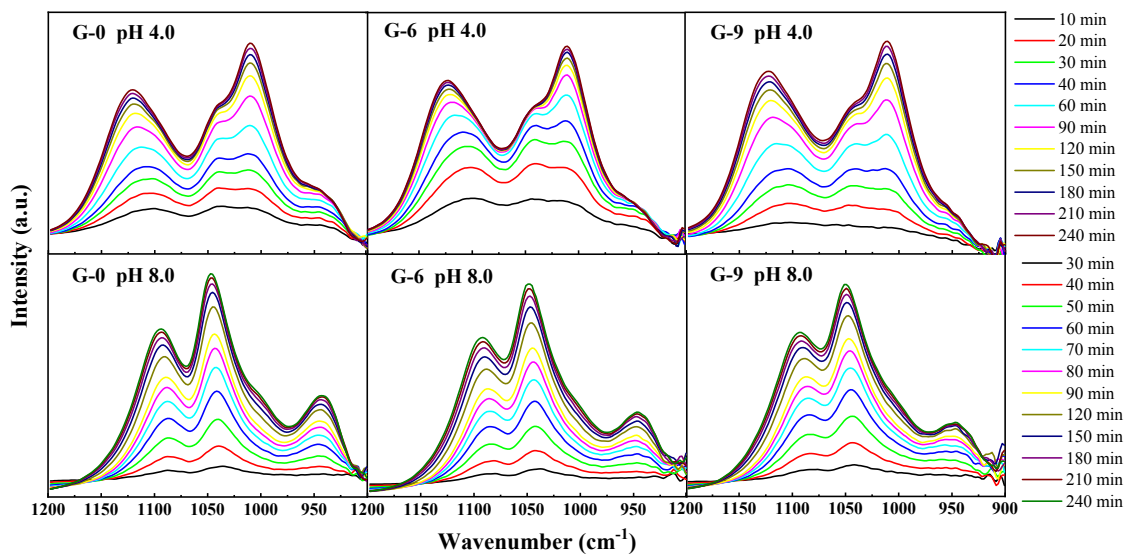
Fig. S6 SEM images of goethite and Al-substituted goethites



**Fig. S7 Histograms of G-0 (a, b), G-6 (c, d) and G-9 (e, f) particle length and width distributions**



**Fig. S8 Time-dependent ATR-FTIR spectra of adsorbed phosphate**



Time-dependent ATR-FTIR spectra of adsorbed phosphate on G-0, G-6 and G-9 at pH 4.0 and 8.0 in 0.1 M KNO<sub>3</sub> and with an initial phosphate concentration of 100 μM and a time range of 10 to 240 min.

## **Two-dimensional correlation spectroscopy (2D-COS) of phosphate adsorption**

The overlapping vibrational peaks in the time dependent ATR-FTIR spectra can be distinguished with 2D-COS analysis. Synchronous and asynchronous spectra can be obtained from 2D-COS analysis. The *synchronous plot* is analyzed by identifying the diagonal auto peaks and the off-diagonal cross peaks. The former provide information about peaks responsible for the major spectral variation as an external perturbation (in this case interaction time), while the latter are a measure of the correlated response to the perturbation at two different wavenumbers. The *asynchronous plot* does not contain auto peaks, but the cross peaks show the uncorrelated peak responses, which are partly or completely out-of-phase depending on the perturbation.

Fig. S9 and S10 show the synchronous (panels a and c) and asynchronous (panels b and d) 2D correlation contour maps of the ATR-FTIR spectra for phosphate adsorption on Al-substituted goethites at both pH 4.0 (Fig. S9a-b) and 8.0 (Fig. S9c-d) in 0.1 M KNO<sub>3</sub>. The red and blue areas represent the positive and negative peaks, respectively. All auto peaks (synchronous map) along the diagonal are positive and their intensity changes at the same direction based on the off-diagonal positive cross peaks. Strong auto peaks locate at 1127 and 1010 cm<sup>-1</sup> at pH 4.0 (Fig. S9a and c) and 1097, 1047 and 940 cm<sup>-1</sup> at pH 8.0 (Fig. S10a and c) are observed, revealing that these bands are the major changes in intensities under perturbation at each pH. The cross peaks in synchronous maps reflect the bands with coupled, or related origins,

and the positive sign suggests the same direction of change in band intensity, these indications are summarized in Table S4 and S5.

The sequential order of intensity changes between two bands at  $\nu_1$  and  $\nu_2$  could be obtained from the sign of synchronous correlation  $\Phi(\nu_1, \nu_2)$  and asynchronous correlation  $\Psi(\nu_1, \nu_2)$  under the well-established principles described by Noda and Ozaki (2005)<sup>11</sup>. Briefly, the change in the spectral intensity at  $\nu_1$  band occurs prior to that at  $\nu_2$  if  $\Phi(\nu_1, \nu_2)$  and  $\Psi(\nu_1, \nu_2)$  have the same sign, whereas the order is reversed if  $\Phi(\nu_1, \nu_2)$  and  $\Psi(\nu_1, \nu_2)$  have the opposite sign. The changes at  $\nu_1$  and  $\nu_2$  occur simultaneously if  $\Psi(\nu_1, \nu_2)$  is zero. Asynchronous analysis is very useful in enhancing the resolution and separating the overlapped bands arising from different species. As suggested by Norén and Persson (2007)<sup>12</sup>, pairs of peaks with positive synchronous correlation but no asynchronous response arise from one common complex. On the basis of these criteria, three groups of frequencies can be resolved in Fig. S9 and S10: (a) 1127 and 1010  $\text{cm}^{-1}$ ; (b) 1100, 1050 and 935  $\text{cm}^{-1}$ ; and (c) 1080, 1039 and 956  $\text{cm}^{-1}$ , which correspond to three different surface complexes. Based on the sign of the combination of synchronous correlation and asynchronous correlation (Table S4 and S5), it may be concluded that the changes in the spectral intensity of group (b) occurred prior to group (a) at pH 4.0, and those of group (c) took place preferentially to group (a) and (b).

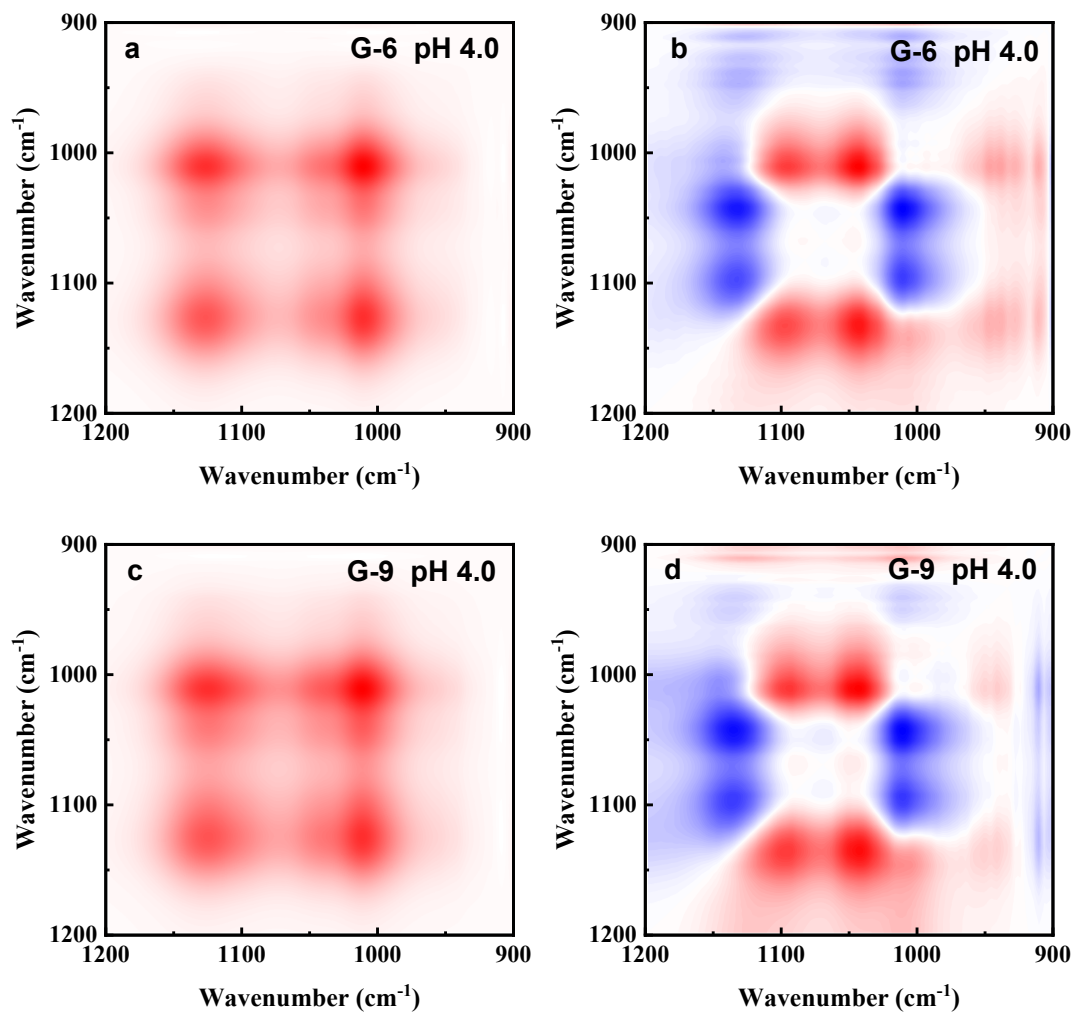


**Fig. S9** Synchronous (a, c) and asynchronous (b, d) contour plots obtained from the dynamic spectra with 100  $\mu\text{M}$  phosphate adsorption on G-6 (a, b) and G-9 (c, d) from 10 to 240 min at pH 4.0 with the salt concentration of 0.1 M  $\text{KNO}_3$ . The red and blue areas represent the positive and negative peaks, respectively.

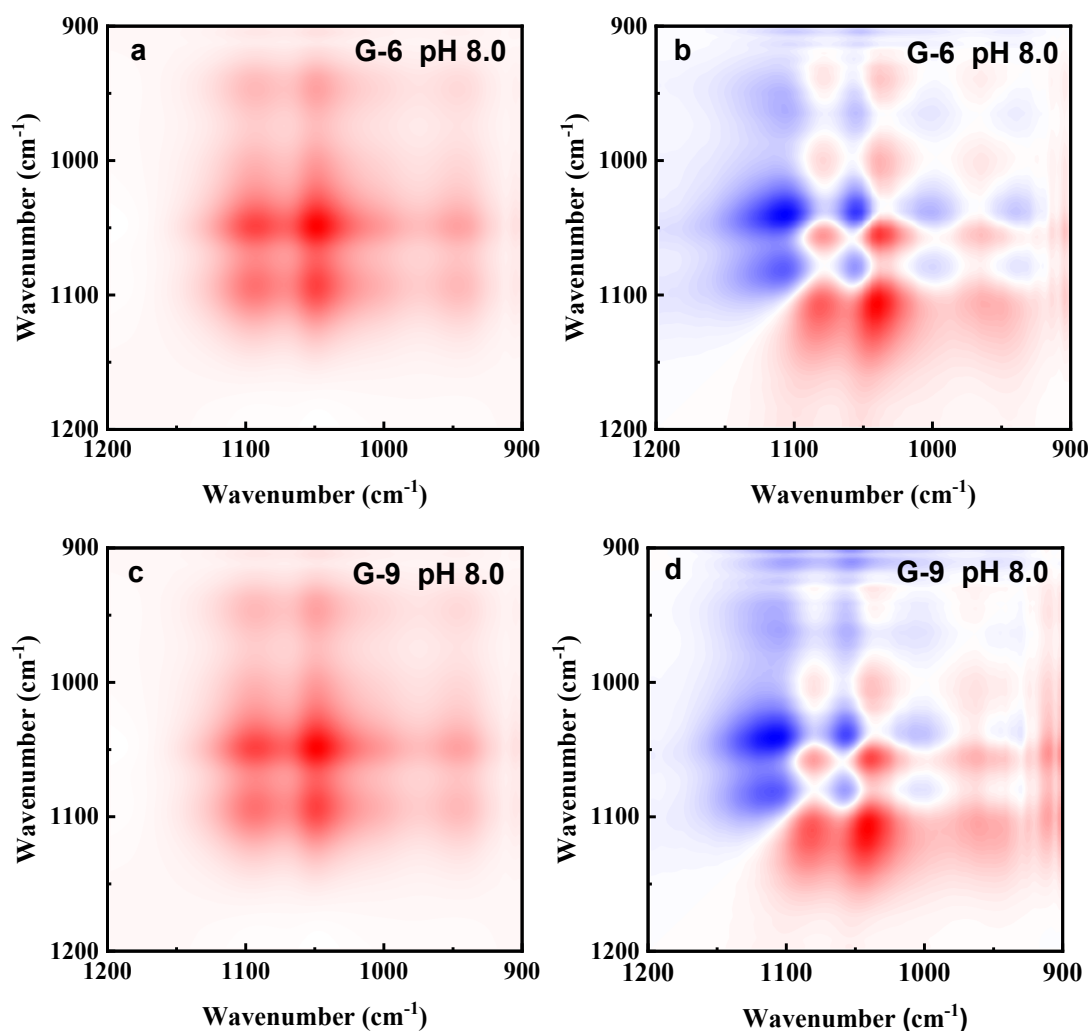


**Fig. S10** Synchronous (a, c) and asynchronous (b, d) contour plots obtained from the dynamic spectra with 100  $\mu\text{M}$  phosphate adsorption on G-6 (a, b) and G-9 (c, d) from 10 to 240 min at pH 8.0 with the salt concentration of 0.1 M  $\text{KNO}_3$ . The red and blue areas represent the positive and negative peaks, respectively.

**Table S4** Two-dimensional correlation analysis of phosphate adsorption on goethite at pH 4.0 with the increasing time

Wavenumber (cm <sup>-1</sup> )	1127	1100	1050	1010	935
1127	*				
1100	+(+)	*			
1050	+(+)	+	*		
1010	+	+(-)	+(-)	*	
935	+(+)	+	+	+(+)	*

The signs are obtained in the lower-right of the contour plots. The left and right signs in each cell indicate the synchronous and asynchronous responses, respectively. “\*” stands for a synchronous auto peak. “+” represents the positive signal, and “-” represents the negative signal.

**Table S5** Two-dimensional correlation analysis of phosphate adsorption on goethite at pH 8.0 with the increasing time

Wavenumber r (cm <sup>-1</sup> )	1127	1100	1080	1055	1039	1010	956	935
1127	*							
1100	+	*						
1080	+(+)	+(+)	*					
1055	+	+	+(-)	*				
1039	+(+)	+(+)	+	+(+)	*			
1010	+	+	+(-)	+	+(-)	*		
956	+(+)	+(+)	+	+(+)	+	+(+)	*	
935	+	+	+(-)	+	+(-)	+	+(-)	*

The signs are obtained in the lower-right of the contour plots. The left and right signs in each cell indicate the synchronous and asynchronous responses, respectively. “\*” stands for a synchronous auto peak. “+” represents the positive signal, and “-” represents the negative signal.

## The sensitivity analysis of the fitting of surface charge data

The difference in the charge density may be attributed to difference in site densities and/or  $\log K_H$  values of each site type and/or a difference in inner Stern layer capacitance ( $C_1$ ). In order to find out the main factors that affect the charge density, a sensitivity analysis was performed. The results are shown in Fig. S11. The black curves (covered by red curves) are calculated charge curves of G-0 at different ionic strengths (0.005 M, 0.03 M and 0.1 M) with the parameters in Table 2. With other parameters fixed, the site densities of each type of sites were changed into the corresponding values for G-9. The obtained charge curves (red curves in Fig. S11) almost overlap with the black curves, indicating that the site densities have limited influence on the charge density. The result agrees with a previous study<sup>13</sup> that demonstrated that the fitting of proton adsorption data is rather insensitive to the choice of site density over wide ranges of this parameter. If the site densities of each site type and  $\log K_H$  values of singly coordinated sites were set equal to those of G-9 (see blue curves), the charge density increases somewhat, especially at low pH. Similarly, the charge density also increases as  $C_1$  increases (green curves). Thus, we conclude that an increase in  $\log K_H$  value of singly coordinated sites and the  $C_1$  value have contributed to the slightly larger surface charge densities at a given pH.

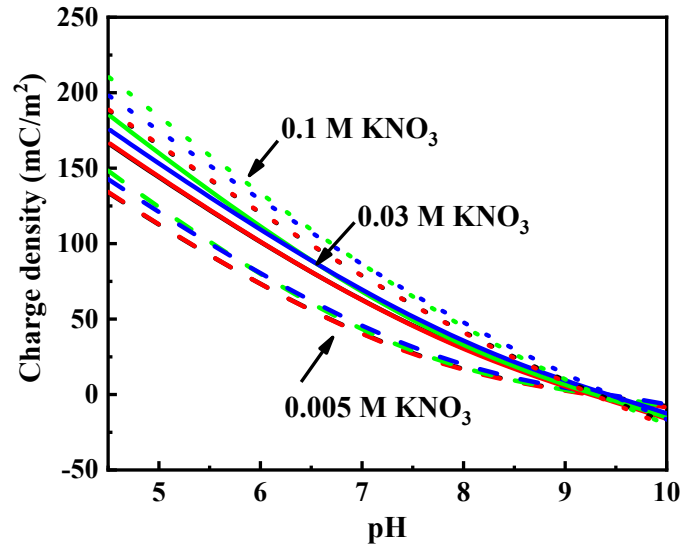


**Fig.S11** The sensitivity analysis of the fitting of surface charge data. Taking G-0 at three different ionic strength (0.005 M, 0.03 M and 0.1 M  $\text{KNO}_3$ ) as an example, black curves (covered by red curves) are calculated with the parameters of G-0 in Table 2 (MS); red curves are calculated by changing the site densities of singly and triply coordinated sites equal to those for G-9, with other parameters kept the same as G-0; blue curves are calculated by changing the site densities of each site types and  $\log K_H$  values of singly coordinated sites equal to those for G-9; green curves are calculated by only changing the inner Stern layer capacitance ( $C_1$ ) the same as G-9.

## References

1. M. Alvarez, E. H. Rueda and E. E. Sileo, Simultaneous incorporation of Mn and Al in the goethite structure, *Geochim. Cosmochim. Acta*, 2007, **71**, 1009-1020.
2. N. Kaur, B. Singh and B. J. Kennedy, Dissolution of Cr, Zn, Cd, and Pb single- and multi-metal-substituted goethite: relationship to structural, morphological, and dehydroxylation properties, *Clays Clay Miner.*, 2010, **58**, 415-430.
3. J. Kabai, Determination of specific activation energies of metal oxides and metal oxide hydrates by measurement of the rate of dissolution, *Acta Chim. Acad. Sci. Hung.*, 1973, **78**, 57-73.
4. U. Schwertmann, The influence of aluminium on iron oxides: IX. Dissolution of Al-goethites in 6 M HCl, *Clay Miner.*, 1984, **19**, 9-19.
5. M. Landers, R. J. Gilkes and M. Wells, Dissolution kinetics of dehydroxylated nickeliferous goethite from limonitic lateritic nickel ore, *Appl. Clay Sci.*, 2009, **42**, 615-624.
6. M. Ducher, M. Blanchard, D. Vantelon, R. Nemausat and D. Cabaret, Probing the local environment of substitutional Al in goethite using X-ray absorption spectroscopy and first-principles calculations, *Phys. Chem. Miner.*, 2016, **43**, 217-227.
7. W. Tan, L. Koopal, L. Weng, W. Van Riemsdijk and W. Norde, Humic acid protein complexation, *Geochim. Cosmochim. Acta*, 2008, **72**, 2090-2099.
8. J. Murphy and J. P. Riley, A modified single solution method for the determination of phosphate in natural waters, *Anal. Chim. Acta*, 1962, **27**, 31-36.
9. P. Venema, T. Hiemstra, P. G. Weidler and W. H. van Riemsdijk, Intrinsic proton affinity of reactive surface groups of metal (hydr) oxides: Application to iron (hydr) oxides, *J. Colloid Interface Sci.*, 1998, **198**, 282-295.
10. R. Rahnemaie, T. Hiemstra and W. H. van Riemsdijk, A new surface structural approach to ion adsorption: Tracing the location of electrolyte ions, *J. Colloid Interface Sci.*, 2006, **293**, 312-321.
11. I. Noda and Y. Ozaki, Two-dimensional correlation spectroscopy: Applications in vibrational and optical spectroscopy, John Wiley & Sons, 2005.
12. K. Norén and P. Persson, Adsorption of monocarboxylates at the water/goethite interface: The importance of hydrogen bonding, *Geochim. Cosmochim. Acta*, 2007, **71**, 5717-5730.
13. D. A. Sverjensky, Standard states for the activities of mineral surface sites and species. *Geochim. Cosmochim. Acta*, 2003, **67**, 17-28.